THE JOURNAL OF PHYSICAL CHEMISTRY C

Article

pubs.acs.org/JPCC

Understanding the Nucleation and Growth of Metals on TiO_2: Co Compared to Au, Ni, and Pt

Randima P. Galhenage,[†] Hui Yan,[†] Samuel A. Tenney,[†] Nayoung Park,[‡] Graeme Henkelman,[‡] Peter Albrecht,[§] David R. Mullins,[§] and Donna A. Chen*[,†]

[†]Department of Chemistry and Biochemistry, University of South Carolina, Columbia, South Carolina 29208, United States

[‡]Department of Chemistry and Biochemistry, University of Texas, Austin, Texas 78712, United States

[§]Oak Ridge National Laboratory, Oak Ridge, Tennessee 37831, United States

ABSTRACT: The nucleation and growth of Co clusters on vacuum-annealed (reduced) and oxidized TiO_2(110) have been studied by scanning tunneling microscopy (STM), X-ray photoelectron spectroscopy (XPS), and density function theory (DFT) calculations. On vacuum-annealed TiO_2(110), the Co clusters grow as three-dimensional islands at coverages between 0.02 and 0.25 ML, but the cluster heights range from ~3 to 5 Å, indicating that the clusters are less than three layers high. In addition to the small cluster sizes, the high nucleation density of the Co clusters and lack of preferential nucleation at the step edges demonstrate that diffusion is slow for Co atoms on the TiO_2 surface. In contrast, deposition of other metals such as Au, Ni, and Pt on TiO_2 results in larger cluster sizes with a smaller number of nucleation sites and preferential nucleation at step edges. XPS experiments show that Co remains in the metallic state, and there is little reduction of the titania surface by Co. A comparison of the metal−titania binding energies calculated by DFT for Co, Au, Ni, and Pt indicates that stronger metal−titania interactions correspond to lower diffusion rates on the surface, as observed by STM. Furthermore, on oxidized TiO_2 surfaces, the diffusion rates of all of the metals decrease, resulting in smaller cluster sizes and higher cluster densities compared to the growth on reduced TiO_2. DFT calculations confirm that the metal−titania adsorption energies are higher on the oxidized surfaces, and this is consistent with the lower diffusion rates observed experimentally.

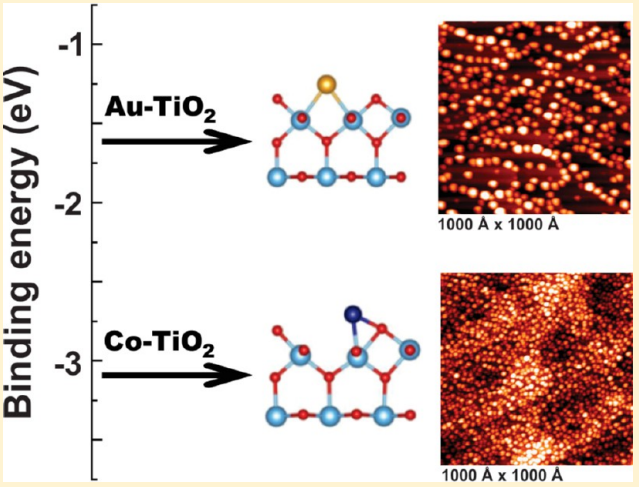

INTRODUCTION

Understanding the growth of metals on oxide surfaces is of critical importance for a wide variety of applications, including those involving heterogeneous catalysis, electronic devices, and gas sensors.[1−4] In catalysis, the number of active sites depends on the exposed surface area of the supported metal clusters, and therefore the growth mode of the metal clusters is crucial for determining the activity of the supported clusters.[2,5,6] In the fabrication of gas sensors and other electronic devices, the ability of metal films to adhere to the oxide substrate depends on the nature of bonding at the metal−oxide interface.[3,7−9]

Co is an important Fischer−Tropsch catalyst for the synthesis of hydrocarbons from CO and H_2 (syngas).[10,11] The attractiveness of Co as a catalyst for the Fischer−Tropsch reaction stems from its high activity,[10−12] high selectivity for longer chain hydrocarbons,[13] and low activity for the undesired water-gas shift side reaction.[11,14] Furthermore, titania is a preferred support for the Co-based Fischer−Tropsch catalysts[12,15−22] due to its excellent thermal stability under reaction conditions and good mechanical properties.[23] The Co−TiO_2 system has also been used for other industrially relevant catalytic processes, including the steam reforming of ethanol,[24] preferential oxidation of CO in hydrogen,[25] and oxidative dehydrogenation of ethane.[26] The nature of the Co−titania interface is believed to influence the chemical activity of the supported Co clusters. For example, the number of active sites is altered by the extent of sintering or agglomeration of the clusters during heating as well as the initial wetting ability of the Co on titania. While strong Co−titania interactions favor higher activity through greater dispersion, the formation of a Co−titanate compound is known to deactivate Co catalysts.[14] It has also been reported that this interfacial reaction, which occurs during reduction with H_2, inhibits the reduction of Co.[27] Previous studies of Co on titania catalysts report strong metal−support interaction (SMSI) effects, such as the decreased adsorption of CO and H_2 after heating the system in a reducing environment.[19,20,28,29] Recent investigations of Co on TiO_2(110) from our group show that the Co clusters become

Received: February 4, 2013
Revised: March 13, 2013
Published: March 19, 2013

   dx.doi.org/10.1021/jp401283k | J. Phys. Chem. C 2013, 117, 7191−7201

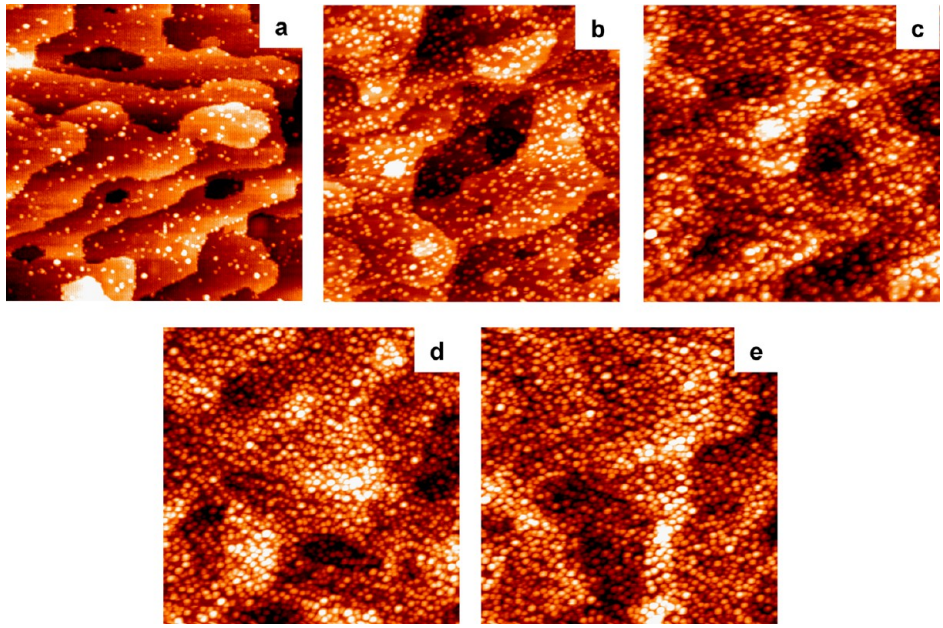

Figure 1. STM images of the following coverages of Co deposited on TiO_2(110) at room temperature: (a) 0.02, (b) 0.06, (c) 0.13, (d) 0.19, and (e) 0.25 ML. All images are 1000 Å × 1000 Å.

partially encapsulated by titania upon heating in vacuum,[30] and other investigations of Co on TiO_2(110) observe decreased Co photoemission upon annealing,[29] which is also consistent with encapsulation.

In order to better understand the growth of Co on titania and the nature of the Co−titania interfacial interactions, we have studied vapor-deposited Co clusters on rutile TiO_2(110) using techniques such as scanning tunneling microscopy (STM) and X-ray photoelectron spectroscopy (XPS) under ultrahigh vacuum (UHV) conditions. The deposition of Co on titania at room temperature results in greater cluster densities and smaller cluster sizes compared to other transition metals grown on TiO_2(110). Co remains predominantly metallic and does not induce significant reduction of the titania support. Upon heating the surface, the Co clusters undergo sintering to form larger clusters. Density functional theory (DFT) studies were carried out to calculate the binding energy of a single metal atom on vacuum-annealed (reduced) TiO_2 for Co as well as other transition metals like Au, Ni, and Pt. This binding energy scales with the strength of oxygen−metal bonds formed on close-packed single crystal surfaces of the metals. The relative cluster sizes and densities for various metals on TiO_2 are successfully predicted based on the metal−titania binding energies: stronger metal−titania binding results in slower diffusion rates and smaller clusters with higher cluster densities. Furthermore, diffusion rates for metals deposited on oxidized TiO_2 were lower than on reduced TiO_2 for all four metals (Au, Ni, Pt, Co) due to the formation of strong admetal−oxygen bonds.

EXPERIMENTAL METHODS

All experiments were conducted in two ultrahigh vacuum chambers. The first chamber has a base pressure of $<5 \times 10^{-11}$ Torr and is equipped with a variable-temperature scanning tunneling microscope (Omicron, VT-25), hemispherical analyzer (Omicron, EA125) for X-ray photoelectron and low-energy ion scattering experiments, low-energy electron diffraction optics (Omicron SPEC3), and a quadrupole mass spectrometer (Leybold-Inficon Transpector 2). A more detailed description of the chamber, as well as sample heating and metal deposition procedures, can be found elsewhere.[31−36] The second chamber has a base pressure of $\lesssim 2 \times 10^{-10}$ Torr and was used to conduct soft X-ray photoelectron spectroscopy (sXPS) experiments on the U12a beamline at the National Synchrotron Light Source.[37−40] The rutile TiO_2(110) crystals (Princeton Scientific) were cleaned by several cycles of Ar ion sputtering at 1 kV for 20 min followed by annealing to 950−1000 K for 1−3 min. Preferential loss of oxygen from the crystals through this treatment resulted in crystals that were reduced and sufficiently conductive for STM and XPS experiments. All TiO_2(110) surfaces were subjected to this treatment unless otherwise specified, and these surfaces are referred to as vacuum-annealed or reduced TiO_2(110). Surface cleanliness and order were confirmed by a combination of XPS, STM, and LEED. Temperatures were measured by type K or C thermocouples spot-welded to the backplate of the crystal and independently calibrated with an infrared pyrometer.[31]

In the first chamber, metals were deposited via a commercial metal evaporator (Oxford Applied Research, EGC04) using electron beam heating of pure Co, Pt, and Ni rods and Au pellets contained in a Mo crucible. In the second chamber, Co was evaporated from a 0.25 mm pure Co wire (99.995%, ESPI) wrapped around a 0.50 mm W wire (ESPI), through which current was passed to heat the Co. Metal coverages and fluxes were measured by a quartz crystal microbalance, which was independently calibrated.[30] Deposition rates for all of the metals were ∼0.1 ML/min, where 1 monolayer (ML) is defined by the packing densities of the Co(0001), Pt(111), Ni(111), and Au(111) surfaces. Oxygen (Matheson, 99.997%) exposures were carried out at room temperature with a pressure rise of 1×10^{-7} Torr for 5 min using a stainless steel directed dosing tube positioned 5 mm from the face of the crystal.

XPS data for the Co(2p) region were collected with an Al Kα source using a 0.2 s dwell time and 0.03 eV step size. The Ti(2p) region was collected with a photon energy of 600 eV, step size of 0.1 eV, and dwell time of 0.1 s. STM studies were

dx.doi.org/10.1021/jp401283k | J. Phys. Chem. C 2013, 117, 7191−7201

conducted at a sample bias of +2.3 V and a tunneling current of 0.05−0.1 nA with electrochemically etched tungsten tips.[33] Measurements of cluster heights in the STM images were carried out with an in-house analysis program that has been described elsewhere.[30,41] Cluster heights are used as measure of cluster size since the diameters are known to be overestimated due to tip convolution effects.[30,33]

COMPUTATIONAL METHODS

Density functional theory calculations[42,43] of metal binding to TiO_2 were performed with the Vienna Ab-initio Simulation Package.[44,45] Core electrons were described by projector augmented-wave potentials[45,46] and valence electrons with a plane wave basis using an energy cutoff of 300 eV. Electron correlation was modeled within the generalized gradient approximation using the PW91 functional of Perdew and Wang.[47] A Dudarev +U correction of U_{eff} = 4 eV was applied to the Ti d states.[48,49] All calculations were spin polarized. The Brillouin zone was sampled at the Γ-point. A dipole correction was applied in the direction normal to the TiO_2 surface.

The calculated lattice constant of bulk rutile TiO_2 (a = 4.68 Å, c = 3.03 Å, c/a = 0.64) was found to be in good agreement with literature values.[50] To study the binding of metal atoms, we used a rutile (110) slab structure having three stoichiometric layers and a 3 × 2 surface supercell. We prepared a reduced TiO_2 surface by removing one bridging oxygen atom from a stoichiometric slab and an oxidized surface by adding an oxygen atom on top of the 5-fold (5f) Ti site. The bottom TiO_2 layer was held fixed in bulk lattice positions during geometry optimization, and the topmost two layers were free to relax. Binding energies of various metal atoms on the TiO_2 (110) slabs were calculated as $E_b = E_{metal/slab} - E_{metal} - E_{slab}$, with $E_{metal/slab}$, E_{metal}, and E_{slab} being the energy of the bound system, metal in gas phase, and TiO_2 slab, respectively.

RESULTS

Scanning tunneling microscopy experiments were carried out on various coverages of Co deposited on TiO_2(110) at room temperature (Figure 1). For the lowest coverage of 0.02 ML, relatively small clusters are formed with an average height of 3.3 ± 0.9 Å and a cluster density of 5.27 × 10^{12} clusters/cm^2 (Figure 1a). Although three-dimensional clusters are grown on the surface, many of the clusters are only 1−2 atomic layers thick, suggesting strong interactions between the TiO_2 support and the Co clusters. Furthermore, there is no preference for the clusters to reside at the step edges, which are the high coordination sites, and this implies that the diffusion length of the Co atoms on TiO_2 is shorter than the distance between steps on the titania surface. As the coverage is increased to 0.06 and 0.13 ML, the number of clusters on the surface and the average cluster height increases, with the height reaching 4.4 ± 1.2 Å at 0.13 ML (Figure 1b,c). These same trends continue as the Co coverage is increased to 0.19 ML and then 0.25 ML, where the surface appears to be completely covered with clusters with an average height of 5.2 ± 1.6 Å (Figure 1d,e).

A quantitative comparison of cluster height and densities as a function of coverage is shown in Figure 2. From 0.02 to 0.06 ML, the number of clusters on the surface increases linearly, with the number of clusters increasing by a factor of 1.8 (Figure 2a). Between 0.06 and 0.19 ML, the clusters density increases less sharply as the surface becomes covered with clusters, and therefore the probability of an incoming Co atom joining an existing cluster becomes high despite the short diffusion length of Co on TiO_2. In the highest coverage regime of 0.19−0.25 ML, the number of clusters nearly plateaus, presumably because there is little exposed titania on which new clusters can nucleate, and consequently the incoming Co atoms are likely to contribute to the growth of existing clusters. Although the average heights of the clusters also increase nearly linearly from the lowest to highest coverage studied (Figure 2b), the total increase in height between 0.02 and 0.25 ML is only ∼2 Å, which roughly corresponds to a single atomic layer.

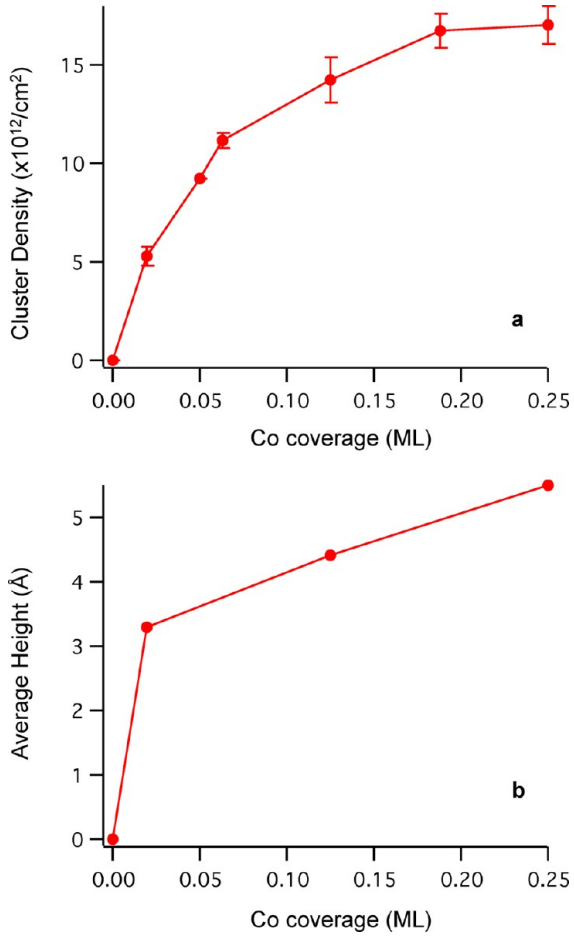

Figure 2. Cluster densities (a) and average cluster heights (b) as a function of increasing Co coverage on TiO_2(110). The error bars for the cluster densities are the standard deviations from counting the clusters in three 1000 Å × 1000 Å images from the same experiment except for the 0.19 ML clusters, where only two images were counted.

At a coverage of 0.02 ML of Co, the height distribution is very narrow, with 80% of the clusters in the 2−4 Å range and 20% in the 4−6 Å range (Figure 3). As the coverage is increased to 0.13 ML, the distribution becomes slightly broader; larger clusters appear with heights of 8 Å, and only 40% of the clusters are 2−4 Å high. Furthermore, at 0.25 ML, clusters as large as 10 Å are observed, and the smaller 2−4 Å clusters comprise <20% of the total distribution. The broadening of the size distribution with increasing coverage is explained as follows: at the higher coverages, incoming Co atoms can both nucleate new clusters, which contribute to the smallest cluster sizes, or become incorporated into existing clusters, which contributes to the larger cluster sizes. In contrast, at the lower coverages, almost all of the Co atoms nucleate new clusters because the diffusion length is not large

dx.doi.org/10.1021/jp401283k | J. Phys. Chem. C 2013, 117, 7191−7201

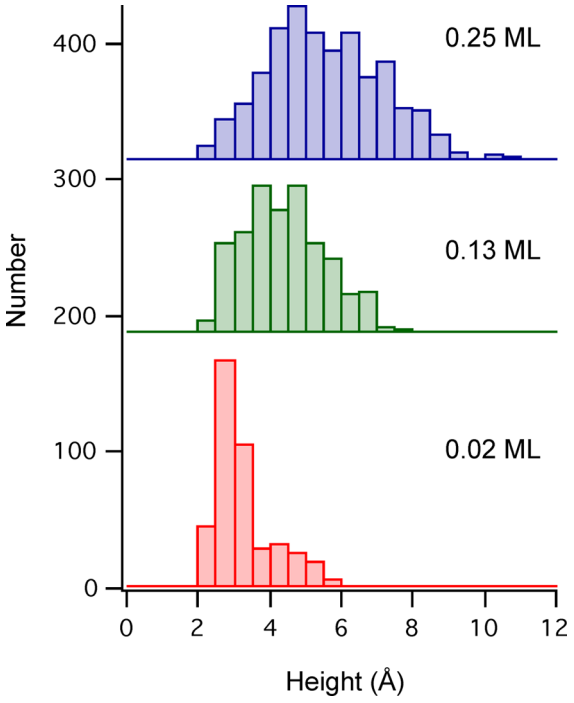

Figure 3. Cluster height distributions for various coverages of Co deposited on TiO_2 at room temperature. Heights were determined from STM images using an in-house cluster measurement program, and the following image sizes were used for the analysis: 1000 Å × 1000 Å for 0.02 ML, and 500 Å × 1000 Å for 0.13 and 0.25 ML.

enough for these atoms to reach existing clusters. In general, our group has observed that the size distribution for metals grown on TiO_2 becomes narrower as the diffusion length decreases; for example, on a TiO_2 surface that was intentionally made defective by heating to induce partial reconstruction of the surface, the deposition of Cu clusters resulted in a more uniform size distribution than on stoichiometric $TiO_2(110)$-(1 × 1).[51,52] The same behavior has been reported for the growth of Pd,[53] Ag,[54] and Pt[55] on reconstructed $TiO_2(110)$-(1 × 2) surfaces.

The most striking feature of the growth of Co on TiO_2 is that the nucleation density for Co is much higher than for other mid-late transition metals on $TiO_2(110)$,[33,36,52,54,56−64] implying a lower diffusion rate for Co on TiO_2. A more direct comparison of the growth of Co with Au, Ni, and Pt is shown in the STM images in Figure 4, where 0.25 ML of each metal is deposited at room temperature. Because the four metals have different rates of diffusion on TiO_2, the resulting cluster sizes and densities are also different, and cluster heights and densities for these surfaces are presented in Table 1. Au clusters (Figure 4a) have the largest average cluster heights of the four metals (12.7 ± 4.3 Å) and the lowest cluster density, indicating that Au atoms have the greatest mobility on TiO_2. Furthermore, the Au clusters exhibit a tendency to reside at the step edges since the Au atoms are able to diffuse across the terraces. Ni atoms diffuse slightly less readily than Au; the average cluster height is smaller (11.1 ± 2.8 Å), and the cluster density for Ni is a factor of 1.7 higher than for Au although the Ni clusters are still preferentially located at step edges (Figure 4b). In the case of Pt, a significant fraction of the clusters appear on the terraces, but the step edge sites are also occupied by clusters (Figure 4c). The average cluster height for Pt decreases to 6.0 ± 2.1 Å, and the cluster density is more than twice that of Ni. The Co

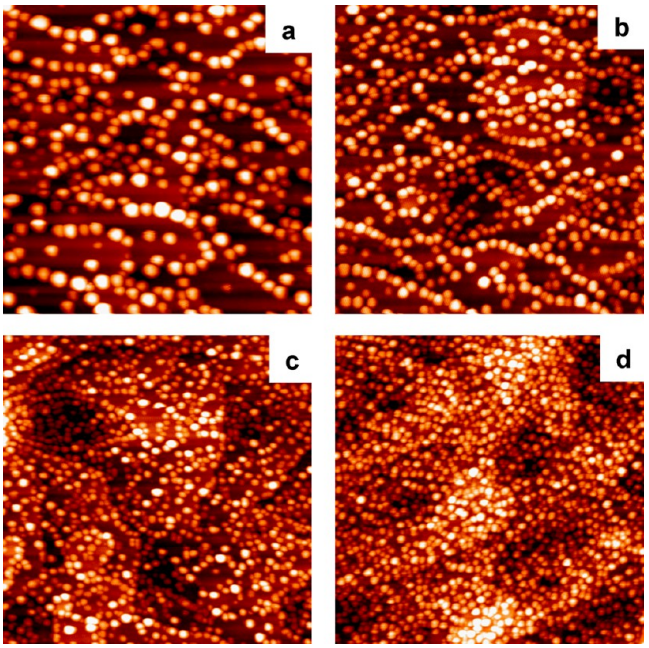

Figure 4. STM images of 0.25 ML of the following metals deposited at room temperature on $TiO_2(110)$: (a) Au, (b) Ni, (c) Pt, and (d) Co. All images are 1000 Å × 1000 Å.

Table 1. Average Cluster Heights and Densities for 0.25 ML of Metal Deposited on Vacuum-Annealed $TiO_2(110)$ at Room Temperature[a]

surface	av height (Å)	cluster density (clusters/cm^2)
0.25 ML Au	12.7 ± 4.3	3.02 × 10^{12}
0.25 ML Ni	11.1 ± 2.8	5.24 × 10^{12}
0.25 ML Pt	6.0 ± 2.1	1.17 × 10^{13}
0.25 ML Co	5.2 ± 1.6	1.63 × 10^{13}

[a]These statistics are based on measurements of all clusters in 1000 × 1000 Å^2 images, which contained a minimum of 300 clusters.

clusters have no preference for nucleation at step edges as well as the smallest cluster height (5.2 + 1.6 Å) and a cluster density that is 1.4 times greater than Pt (Figure 4d).

The binding energies of these metals on $TiO_2(110)$ were calculated by DFT in order to explain the experimental differences in metal nucleation and growth (Table 2). The vacuum-annealed (reduced) TiO_2 surfaces used for the experiments contain ∼7% oxygen vacancies as determined by counting the number of these features in high-resolution STM images, and this number is consistent with the values reported in the literature for similarly prepared $TiO_2(110)$ surfaces.[3] The DFT calculations demonstrate that the metal atoms bind

Table 2. Calculated Metal Binding Energy on the Vacuum-Annealed (Reduced) and the Oxidized $TiO_2(110)$ Surface; Oxygen Binding Energy to the Metal(111) Surface for Au, Ni, and Pt and to (0001) for Co

metal	metal binding energy on reduced TiO_2 (eV)	metal binding energy on oxidized TiO_2 (eV)	oxygen binding energy on metal (eV)
Au	−1.54	−3.89	−3.67
Ni	−1.61	−7.23	−4.02
Pt	−2.28	−6.05	−4.56
Co	−3.07	−8.70	−6.02

dx.doi.org/10.1021/jp401283k | J. Phys. Chem. C 2013, 117, 7191−7201

preferentially at the oxygen vacancies, as also reported in the literature for Pt and Au on TiO_2(110);[65,66] it has generally been observed that for growth on oxide surfaces defects play an important role in the nucleation of the metal clusters.[1] Co binds most strongly to the bridging oxygen vacancy, followed by Pt, Ni, and finally Au. Furthermore, the Co atom binds asymmetrically to one Ti (5f) atom and one bridging oxygen atom, in contrast to the symmetric Ti (5f)−metal−Ti (5f) bond of Pt, Ni, and Au, as shown in Figure 5 (circles, top). The

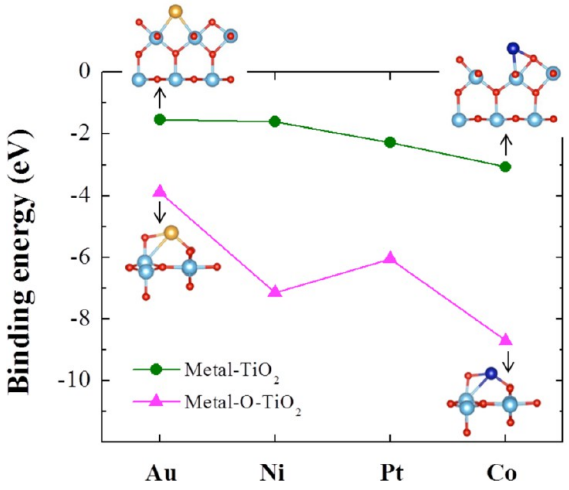

Figure 5. Calculated binding energies of metal atoms on vacuum-annealed (reduced) TiO_2 and oxidized TiO_2 (O-TiO_2) surfaces.

distinct bonding geometry of Co−TiO_2 can be understood in terms of the stronger affinity of Co for oxygen compared with the Pt, Ni, and Au cases. The calculated oxygen binding energies on the (111) surfaces of Au, Pt, and Ni and the (0001) surface of Co are given in Table 2 to illustrate that the metal−titania binding energies are correctly predicted by the admetal−oxygen bond strengths. Likewise, a review article by Campbell on the growth of metals on oxides reports that for metal deposition on alumina the interfacial energy scales with the strength of the admetal−oxygen bond.[1]

From the calculated binding energies of metals, there is a clear trend between binding energy and cluster size/density; specifically, the larger binding energies lead to smaller cluster sizes and higher cluster densities. This behavior can be understood if the rate of diffusion for the metal on titania is assumed to be related to the metal−titania binding energy, with slower rates of diffusion and shorter diffusion lengths associated with strong metal−titania binding. The Bronsted−Evans−Polyani (BEP) relationship suggests that the activation energy barrier for metal diffusion should scale with the adsorption energy of the metal.[67−69] According to the BEP equation, the change in activation energy is equal to a constant times the change in reaction energy for reactions of the same type, and this relationship has been successfully applied to understanding the elementary steps in surface reactions.[67−72] Thus, the activation energies obtained from transition state theory can be directly determined from the more easily calculated thermodynamic properties.[69] More recent work by Norskov and co-workers have shown through DFT calculations that there is a "universal" linear relationship between the activation energy of reaction and the adsorption energies of the atomic species for the dissociation of diatomic molecules (N_2, CO, NO, O_2) on many transition metal surfaces.[73,74] Other DFT investigations have also demonstrated this same relationship between activation energy of reaction and adsorption energies for C−H bond breaking in ethylene,[75] CO dissociation,[76] and N_2 dissociation.[74] Consequently, the rate of diffusion of the metal atoms on the surface should decrease with increasing metal−titania binding. The calculated binding energies in Table 2 are consistent with the diffusion rates for the metals on TiO_2 following the order of Au > Ni > Pt > Co for diffusion rates. The metals with the greatest mobility on the surface exhibit the largest cluster sizes, the smallest cluster densities, and the

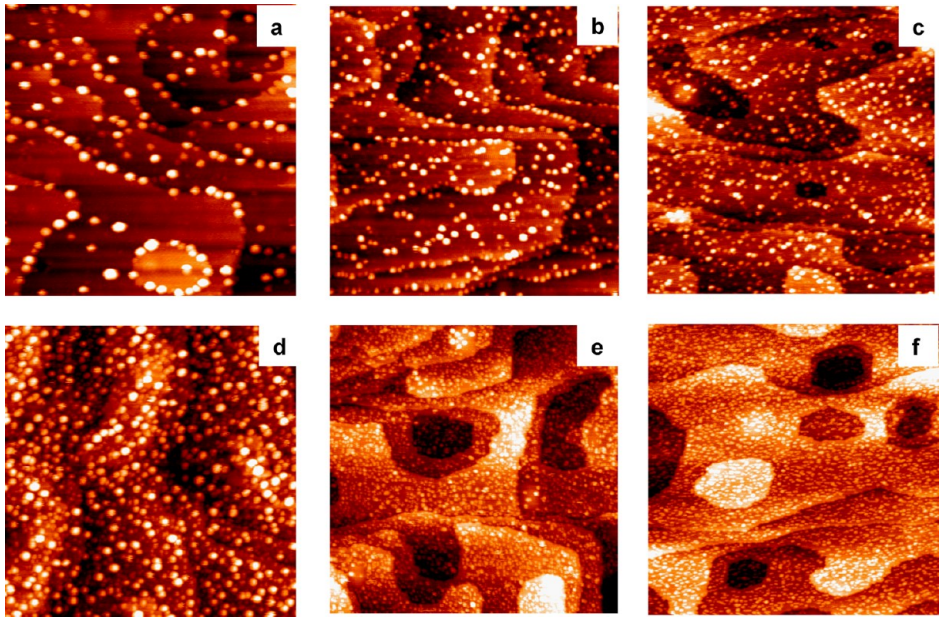

Figure 6. STM images of 0.05 ML of the following metals deposited on vacuum-annealed TiO_2(110) (a, Au; b, Ni; c, Co) and TiO_2 exposed to O_2 at 295 K: (d, Au; e, Ni; f, Co). All metals were deposited at room temperature, and images are 1000 Å × 1000 Å.

dx.doi.org/10.1021/jp401283k | J. Phys. Chem. C 2013, 117, 7191−7201

greatest tendency for the clusters to occupy the high-coordination step edge sites.

The growth of Co, Au, and Ni is substantially altered when the vacuum-annealed TiO_2 surface is exposed to O_2 at 295 K before metal deposition. XPS studies report that this oxygen treatment decreases the Ti^{3+} low binding energy shoulder at ~458 eV in the Ti($2p_{3/2}$) spectrum. The oxidation process is proposed to involve O_2 dissociation at oxygen vacancies and subsequent filling of these vacancies by oxygen adatoms, leaving the remaining oxygen adatoms on the surface.[77,78] STM images in Figure 6 illustrate that for 0.05 ML coverages of various metals the number of clusters is significantly increased for the oxidized surface compared to reduced TiO_2 in all cases. Similarly, the average cluster heights are all smaller for deposition on oxidized TiO_2 compared to the reduced surface. The changes in the cluster sizes and densities (Table 3) suggest

Table 3. Average Cluster Heights and Densities for 0.05 ML of Metal Deposited at Room Temperature on Vacuum-Annealed (Reduced) TiO_2(110) and TiO_2(110) Exposed to O_2 at 295 K (Oxidized, O-TiO_2)[a]

surface	av height (Å)	cluster density (clusters/cm^2)
0.05 ML Co/TiO_2	3.7 ± 1.2	9.32 × 10^{12}
0.05 ML Co/O-TiO_2	3.0 ± 0.4	1.57 × 10^{13}
0.05 ML Au/TiO_2	8.0 ± 2.7	1.88 × 10^{12}
0.05 ML Au/O-TiO_2	4.8 ± 2.3	1.16 × 10^{13}
0.05 ML Ni/TiO_2	4.4 ± 1.5	5.44 × 10^{12}
0.05 ML Ni/O-TiO_2	2.7 ± 0.6	1.42 × 10^{13}

[a]These statistics are based on measurements of all clusters in 500 × 1000 Å^2 or 1000 × 1000 Å^2 images, which included 180−940 clusters.

that diffusion is inhibited on the oxidized surface due to stronger metal−support interactions. The most pronounced difference is observed for Au, given that the cluster density on the oxidized surface increases by a factor of ~6. Both Ni and Co exhibit smaller changes, with the cluster densities increasing by a factor of only 2.6 or 1.7, respectively, on oxidized TiO_2. Thus, Au, which diffuses most readily on reduced TiO_2 shows the most pronounced changes in growth. DFT calculations were conducted to compare the binding energies on the oxidized and reduced TiO_2 surfaces (Figure 5), and the most stable binding sites of metal atoms on oxidized TiO_2 were adopted from the literature.[79] The calculations demonstrate that the binding energy of the metal is higher on oxidized TiO_2 (O-TiO_2) in all cases. Moreover, the binding energy of Au on O-TiO_2 is lower than that of Ni or Co, and this reflects the experimental behavior in which the Au clusters grown on O-TiO_2 have greater average heights (4.8 ± 2.3 Å) than Co (3.0 ± 0.4 Å) or Ni (2.7 ± 1.5 Å), which have similar heights (Table 3). Likewise, STM studies of Ag[80] and Au[79] clusters on oxidized TiO_2(110) have reported stronger bonding of the metal to the oxidized surface compared to the vacuum-annealed surface.[80] This increased binding in the presence of oxygen is reflected in the experimental observation (Figure 6) that the average particle size for all investigated metals is smaller on the oxidized surface.

The difference in metal binding on the reduced and oxidized TiO_2 surfaces can be understood in terms of the relative electronegativities of the metals. The reduced TiO_2 (110) surface is electron-rich, whereas the oxidized TiO_2(110) surface is electron-deficient,[79] and therefore a correlation between the relative electronegativities of the metals and the difference in binding to these surfaces is expected.[81] This was tested by explicitly calculating the binding energy difference, $\Delta E_b = E_b^{oTiO_2} - E_b^{rTiO_2}$, where $E_b^{oTiO_2}$ and $E_b^{rTiO_2}$ are the metal binding energies on the oxidized and reduced TiO_2 (110) surfaces, respectively. Figure 7 shows that the binding energy difference is well-

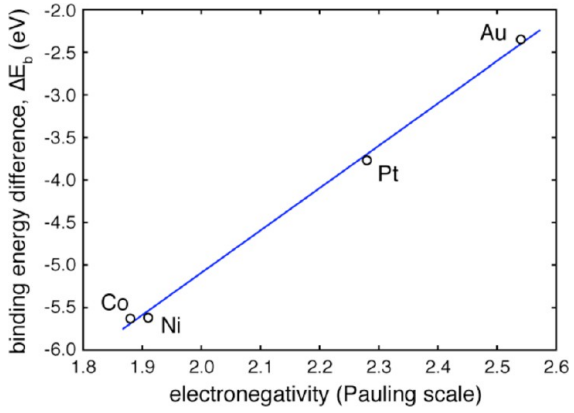

Figure 7. Correlation between the ΔE_b values of metal atoms on TiO_2 with their electronegativities.

correlated with the Pauling electronegativity of the metals.[82] Co, which has the lowest electronegativity, most strongly prefers the oxidizing environment. In contrast, Au has the highest electronegativity and the smallest magnitude of ΔE_b. Although Au has the smallest ΔE_b of the three metals, the ratio of number of clusters on the oxidized compared to TiO_2 surface is the greatest for Au. This behavior is explained by the fact that the reduced TiO_2 surface has very few nucleation sites for Au compared to Ni or Co, and therefore the creation of new nucleation sites on the oxidized surface has the most pronounced effect on the cluster density for Au.

To investigate the interactions between the TiO_2 support and the Co clusters, sXPS experiments were carried out at the U12a beamline at the National Synchrotron Light Source. The surface sensitivity of the experiments was enhanced by using an incident energy of 600 eV so that the photoelectrons have lower kinetic energy than those generated with a conventional Al Kα X-ray source. For these experiments, a higher metal coverage of 2 ML was deposited in order to increase the likelihood of observing the effects of Co−titania interactions. The Ti($2p_{3/2}$) spectrum of the clean TiO_2(110) surface is fit with a main peak at 459.2 eV, which is assigned to Ti^{4+} and accounts for 90% of the total intensity; a smaller feature at 457.7 eV, which is assigned to Ti^{3+}, accounts for the remaining 10% (Figure 8a).[39,83,84] After the deposition of 2 ML of Co (Figure 8b), the Ti^{4+} and Ti^{3+} peaks comprise 80% and 15% of the total intensity, respectively, and a small feature at 456.5 eV appears, which is assigned to Ti^{2+} and accounts for 5% of the intensity. The ~10% decrease in the Ti^{4+} peak compared to clean TiO_2 suggests that a small fraction of Ti^{4+} is reduced by Co. Previous studies of Co clusters annealed at 800 K showed that the clusters were encapsulated by titania,[30] as has also been observed for many other metals such as Pt,[39,84,85] Rh,[39,86] Pd,[87−89] and Ni[32,35,84,90] heated on TiO_2(110) in a reducing environment like UHV. After annealing to 800 K, the Ti($2p_{3/2}$) peak shape is nearly identical to that of the unannealed surface with Ti^{4+}, Ti^{3+}, and Ti^{2+} contributions of 85%, 12%, and 3%, respectively (Figure 8c), and this peak shape is also very similar to the clean TiO_2 surface. Thus, the Co clusters appear to be

dx.doi.org/10.1021/jp401283k | J. Phys. Chem. C 2013, 117, 7191−7201

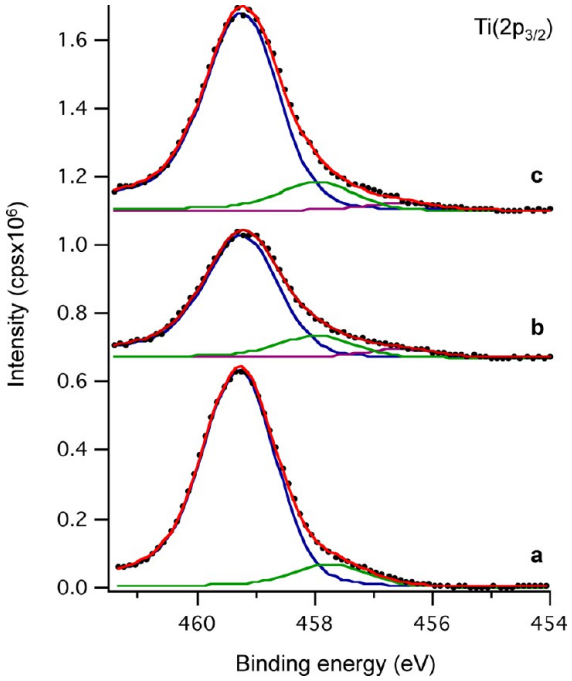

Figure 8. Soft X-ray photoelectron spectroscopy data for the $Ti(2p_{3/2})$ region for (a) clean $TiO_2(110)$ and 2 ML of Co deposited on $TiO_2(110)$ after room temperature deposition (b) and after heating to 800 K for 1 min (c). The incident photon energy was 600 eV.

encapsulated by stoichiometric titania, as also observed for encapsulated Ni clusters,[84] whereas Pt clusters are encapsulated by reduced titania.[39,84,85,91,92]

XPS data for the Co(2p) region indicate that the 0.25 ML Co clusters on TiO_2 consist predominantly of metallic Co (Figure 9). After deposition at room temperature, the Co(2p) peak shape is similar to that of metallic Co with a $Co(2p_{3/2})$ binding energy of 778.5 eV (Figure 9a).[93] However, the peak is slightly broader than what is observed for bulk Co surfaces, with greater intensity in the shoulder around 781 eV. One possibility for the origin of this shoulder is that a small fraction of the Co is oxidized from interaction between the Co clusters and the TiO_2 support; note that Co is not expected to be oxidized by background gases upon deposition in UHV, given that pure metallic Co films have been observed on metal surfaces like Mo in UHV.[94] A similar Co(2p) peak shape has been observed for Co deposited on vanadia thin films, and the spectral intensity around ~781 eV was assigned to a shakeup satellite arising from d−d correlation, rather than oxidation of Co.[95] On the basis of the lower heat of formation of cobalt oxide compared to vanadium oxide, it is unlikely that the Co would be oxidized by the vanadia support,[95] and a similar argument would suggest that Co should not be oxidized by the titania support either. XPS studies of Co thin films grown on Cu and oxidized Cu have attributed the $Co(2p_{3/2})$ shoulder to correlation-induced satellite features, and the intensity of this satellite feature is reported to be very sensitive to film thickness, with greater intensity for thinner films.[96−98] In addition to d−d interaction, the Cu 4s−Co 3d hybridization also contributes to the $Co(2p_{3/2})$ satellite structure for the Co films on Cu. Furthermore, theoretical studies confirm that the d−d correlation is expected to contribute to the satellite structure.[99,100] Therefore, the appearance of the shoulder in the $Co(2p_{3/2})$ spectrum of Co on TiO_2 is not exclusively attributed to oxidation, given that the slight reduction of the titania surface is consistent with the presence of only a small fraction of Co oxide.

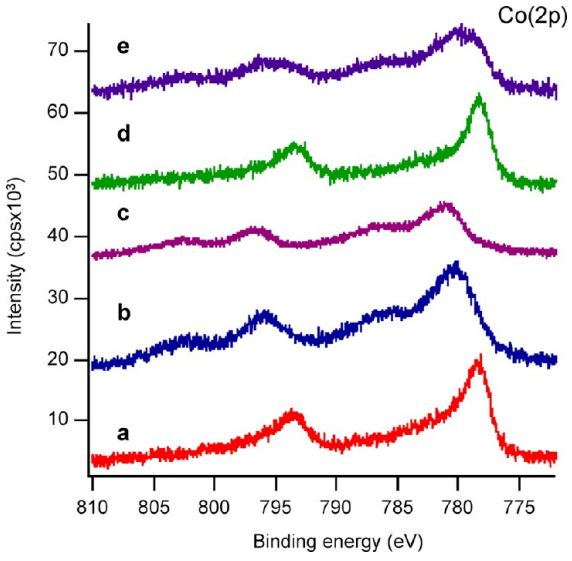

Figure 9. XPS data for the Co(2p) region for 0.25 ML of Co deposited on $TiO_2(110)$ at room temperature: (a) as deposited; (b) exposed to O_2 at room temperature; (c) exposed to air for 24 h; (d) annealed to 800 K for 1 min; and (e) annealed to 800 K for 1 min and exposed to O_2 at room temperature. The O_2 was dosed in UHV at a pressure rise of 1×10^{-7} Torr for 5 min via a directed dosing tube.

In order to understand changes in the Co(2p) spectrum due to oxidation, the 0.25 ML Co clusters were exposed to O_2 at a pressure of 1×10^{-7} Torr for 5 min. The resulting spectrum begins to resembles that of Co oxide[93] as the $2p_{3/2}$ binding energy shifts to 780.5 eV and distinct shoulders appear at a binding energies 5.7 eV higher than the main 2p peaks (Figure 9b). For comparison, the spectrum of 0.25 ML of Co exposed to air for 24 h is shown in Figure 9c to illustrate that the clusters exposed to oxygen in UHV are not fully oxidized. In the spectrum of the Co clusters exposed to air, the $2p_{3/2}$ peak continues to shift to high binding energy (781.1 eV), indicating that this Co surface is more fully oxidized than the one treated in UHV. The Co(2p) spectrum of the clusters annealed to 800 K for 1 min (Figure 9d) shows only a ~20% decrease in the integrated Co intensity, but the $Co(2p_{3/2})$ peak also becomes slightly narrower, which could result from decomposition of the small fraction of Co oxide. Indeed, when the Co clusters are oxidized in UHV and then heated to 800 K, the metallic peak shape is restored as the decomposition of Co oxide occurs at this temperature. However, because the intensity of the shoulder at ~781 eV is dependent on the thickness of the Co overlayers, the changes at 800 K could also be ascribed to a morphological change.[96−98] After annealing to 800 K, the partially encapsulated Co clusters are exposed to O_2 at 295 K (Figure 9e), and there is a significant change in peak shape and a shift in $Co(2p_{3/2})$ binding energy to 779.7 eV. This suggests that the Co clusters become oxidized even after partial encapsulation by titania although the extent of oxidation is not as great as for the unencapsulated Co clusters, based on the smaller shift to higher binding energy.

DISCUSSION

A comparison of Co, Pt, Ni, and Au growth on $TiO_2(110)$ demonstrates that information about the kinetics of cluster

dx.doi.org/10.1021/jp401283k | J. Phys. Chem. C 2013, 117, 7191−7201

growth can be extracted from thermodynamic properties like the admetal−oxygen bond strengths. The relative rates of diffusion increase with decreasing admetal−oxygen bond strengths, and higher diffusion rates lead to larger clusters and lower cluster densities. Co exhibits the lowest diffusion rate since it has the strongest metal−titania bonding, and Au exhibits the highest diffusion rate since it has the weakest metal−titania bonding; Ni and Pt follow the same trend of increasing diffusion rates with weaker metal−TiO_2 bonding. Consequently, cluster sizes increase in the order of Co < Pt < Ni < Au. For Co, its less active neighbors in the periodic table (Rh, Ni) exhibit much higher metal atom diffusion at room temperature,[59,62] implying significantly weaker metal−titania binding compared to Co. Many of the mid-late transition metals have been imaged by STM on TiO_2(110), and the reported spatial distributions also follow the trends predicted by the metal−oxygen bond strengths. Metals like Cu,[58,59] Ag,[57,61,101] Rh,[62] and Pd[53,60] are mobile on the surface at room temperature compared to Pt and Co, which have higher metal−oxygen bond strengths, and therefore the Cu, Ag, Rh, and Pd clusters are preferentially located at the high-coordination step sites. Similarly, metals like Mo[102,103] and Al[104] with stronger metal−oxygen bonds form clusters that show no preference for nucleation at step edges due to the short diffusion lengths.

Diebold and Madey have compared the growth of many transition metals on TiO_2(110) and found that the mode of film growth can also be predicted from thermodynamic properties.[3,4,105] Specifically, the wetting ability of the admetal film depends on the activity of the admetal for reaction with oxygen. Late transition metals like Cu[105] and Au,[56,106] which are not active for reaction with oxygen, grow as three-dimensional islands that do not wet the surface; in contrast, early transition metals like Cr[107] and Mn[108] are active for reaction with lattice oxygen and form flatter islands that wet more of the titania surface. In general, the admetal's activity for reaction with lattice oxygen follows the heat of formation of the oxides per mole of oxygen,[4] similar to the trend observed for reduction of the titania by the admetal. Moreover, a review by Campbell demonstrated that the growth mode for metals on oxides can be predicted from trends in the heats of formation of the admetal oxide.[1] Three-dimensional film growth is expected when $\gamma_o < \gamma_m + \gamma_{m/o}$, where γ_o and γ_m are the surface free energies of the oxide and admetal, respectively, and $\gamma_{m/o}$ is the energy of the admetal−oxide interface. Since the surface free energy of the metal is usually higher than that of oxide,[109] the interfacial energy often controls the mode of film growth, with strong admetal−titania interaction favoring more 2-dimensional growth. Given that the interfacial energy has been shown to scale with the heats of formation for the admetal oxides,[1] two-dimensional growth is expected for admetals with higher heats of formation of the associated admetal oxide.

The general trend observed for transition metals on TiO_2 is that the extent of reduction at the admetal−titania interface increases with the heat of adsorption of oxygen on the admetal.[102] Tanaka and co-workers showed that the heat of adsorption for oxygen follows the standard heat of formation (per metal atom) of the highest oxide,[110] and therefore, the extent of titania reduction by the admetal should increase with increasing heat of formation of the oxide. Fe, which is directly to the left of Co in the periodic table, exhibits greater reduction of the titania surface than Co,[105,111] and the early transition metals such as Cr,[107] V,[4,112] Mo,[113,114] and Mn[108] also reduce titania significantly upon room temperature deposition. In addition, metals in the periodic table that are in or to the left of the Fe group[111] reduce titania while the admetal itself becomes oxidized, and this interfacial reaction enhances wetting ability.[4] For the mid-late transition metals deposited on TiO_2(110) in this study (Au, Pt, Ni, Co), the extent of titania reduction for equivalent coverages of metal also reflects the relative strengths of the admetal−titania bonds even though none of these metals reduce titania substantially.[84] In the case of Au, which has the weakest metal−titania interaction, there is only a ∼3% reduction of Ti^{4+} to Ti^{3+} after deposition. Ni deposition on titania induces a 6% reduction of Ti^{4+} to Ti^{3+} and 3% reduction of Ti^{3+} to Ti^{2+}. Co and Pt, with the strongest metal−oxygen bonds, cause a ∼10% reduction of Ti^{4+} to Ti^{3+} and a ∼5% reduction of Ti^{3+} to Ti^{2+}.

For the deposition of Co on metal oxide surfaces, the extent to which Co is oxidized by the support increases with decreasing heats of formation of the metal oxide. For example, Co becomes oxidized when deposited on niobia thin films[115] and ZnO surfaces,[116−118] but Co remains metallic when deposited on alumina,[115,119,120] vanadia thin films,[95] and the TiO_2(110) single-crystal surfaces reported here. The heats of formation of the metal oxides (per mole oxygen) for the most stable metal oxide follow the order alumina > titania > vanadia > niobia > ZnO.[1,121] Thus, deposited Co is less likely to become oxidized by the support for metal oxides that have the strongest bonds with lattice oxygen. The observed lack of oxidation of Co on TiO_2 is expected based on the heats of formation of titania compared with alumina and vanadia, which also do not oxidize Co clusters.

■ CONCLUSIONS

The growth of Co clusters on TiO_2(110) results in small clusters 3−5 Å high for coverages up to 0.25 ML, accompanied by a relatively high cluster density and no preferential nucleation at step edges. These results demonstrate that Co is less mobile on the surface compared to other mid-late transition metals, which form larger clusters and nucleate at step edges. Room temperature deposition of Co induces only a minor reduction of the titania surface, and Co is not significantly oxidized by the titania support. A comparison of the growth of Au, Ni, and Pt clusters on TiO_2(110) with Co at the same coverage demonstrates that Co forms the smallest clusters and highest cluster densities due to the lowest rates of the diffusion. DFT calculations for the binding energies of these metals on titania show that the diffusion rate decreases with metal−titania bond strength, which also follows the binding energy of oxygen on the close-packed metal surfaces. Therefore, the rate of diffusion and corresponding clusters size can be predicted based on the metal−titania and admetal−oxygen binding energies. Co, with the strongest binding, has the greatest diffusion barrier and therefore forms the smallest clusters; Au, with the weakest binding, is the most mobile and result in the largest clusters. On oxidized TiO_2(110) surfaces, diffusion of all four metals is slower due to strong bonding between the metals and surface oxygen.

■ AUTHOR INFORMATION

Corresponding Author

*Phone 803-777-1050; Fax 803-777-9521; e-mail dachen@sc.edu.

Notes

The authors declare no competing financial interest.

■ ACKNOWLEDGMENTS

We gratefully acknowledge financial support from the National Science Foundation (CHE 0845788, CBET-0932991, and CBET-0966956) and the Department of Energy, Basic Energy Sciences (DE-FG02-07ER15842). Research was sponsored by the Division of Chemical Sciences, Geosciences, and Biosciences, Office of Basic Energy Sciences, US Department of Energy, under Contract DE-AC05-00OR22725 with Oak Ridge National Laboratory, managed and operated by UT-Battelle, LLC. Use of the National Synchrotron Light Source, Brookhaven National Laboratory, was supported by the US Department of Energy, Office of Science, Office of Basic Energy Sciences, under Contract DE-AC02-98CH10886.

■ REFERENCES

(1) Campbell, C. T. Ultrathin Metal Films and Particles on Oxide Surface: Structural, Electronic and Chemisorptive Properties. *Surf. Sci. Rep.* **1997**, *27*, 1−111.
(2) Henrich, V. E.; Cox, P. A. *The Surface Science of Metal Oxides*; Cambridge University Press: Cambridge, 1996.
(3) Diebold, U. The Surface Science of Titanium Dioxide. *Surf. Sci. Rep.* **2003**, *48*, 53−230.
(4) Diebold, U.; Pan, J. M.; Madey, T. E. Ultrathin Metal Film Growth on TiO_2(110): An Overview. *Surf. Sci.* **1995**, *333*, 845−854.
(5) Goodman, D. W. Model Studies in Catalysis Using Surface Science Probes. *Chem. Rev.* **1995**, *95*, 523−536.
(6) Bäumer, M.; Freund, H. J. Metal Deposits on Well-Ordered Oxide Films. *Prog. Surf. Sci.* **1999**, *61*, 127−198.
(7) Fu, Q.; Wagner, T. Interaction of Nanostructured Metal Overlayers with Oxide Surfaces. *Surf. Sci. Rep.* **2007**, *62*, 431−498.
(8) Semancik, S.; Cavicchi, R. E. The Use of Surface and Thin Film Science in the Development of Advanced Gas Sensors. *Appl. Surf. Sci.* **1993**, *70−1*, 337−346.
(9) Novak, D.; Garfunkel, E.; Gustafsson, T. Scanning Tunneling Microscopy Study of the Atomic-Scale Structure of TiO_2(110)-(1 × 1). *Phys. Rev. B* **1994**, *50*, 5000−5003.
(10) Withers, H. P.; Eliezer, K. F.; Mitchell, J. W. Slurry-Phase Fischer−Tropsch Synthesis and Kinetic-Studies over Supported Cobalt Carbonyl Derived Catalysts. *Ind. Eng. Chem. Res.* **1990**, *29*, 1807−1814.
(11) Iglesia, E. Design, Synthesis, and Use of Cobalt-Based Fischer−Tropsch Synthesis Catalysts. *Appl. Catal., A* **1997**, *161*, 59−78.
(12) Dry, M. E. Fischer−Tropsch Catalysts. In *Studies in Surface Science and Catalysis: Fischer−Tropsch Technology*; Steynberg, A., Dry, M., Eds.; Elsevier: Amsterdam, 2004; Vol. *152*, pp 533−600.
(13) Coville, N. J.; Li, J. Effect of Boron Source on the Catalyst Reducibility and Fischer−Tropsch Synthesis Activity of Co/TiO_2 Catalysts. *Catal. Today* **2002**, *71*, 403−410.
(14) Jongsomjit, B.; Sakdamnuson, C.; Goodwin, J. G.; Praserthdam, P. Co-Support Compound Formation in Titania-Supported Cobalt Catalyst. *Catal. Lett.* **2004**, *94*, 209−215.
(15) Jacobs, G.; Das, T. K.; Zhang, Y. Q.; Li, J. L.; Racoillet, G.; Davis, B. H. Fischer−Tropsch Synthesis: Support, Loading, and Promoter Effects on the Reducibility of Cobalt Catalysts. *Appl. Catal., A* **2002**, *233*, 263−281.
(16) Li, J. L.; Jacobs, G.; Das, T.; Davis, B. H. Fischer−Tropsch Synthesis: Effect of Water on the Catalytic Properties of a Ruthenium Promoted Co/TiO_2 Catalyst. *Appl. Catal., A* **2002**, *233*, 255−262.
(17) Li, J. L.; Xu, L. G.; Keogh, R.; Davis, B. Fischer−Tropsch Synthesis. Effect of CO Pretreatment on a Ruthenium Promoted Co/TiO_2. *Catal. Lett.* **2000**, *70*, 127−130.
(18) Jongsomjit, B.; Wongsalee, T.; Praserthdam, P. Study of Cobalt Dispersion on Titania Consisting Various Rutile: Anatase Ratios. *Mater. Chem. Phys.* **2005**, *92*, 572−577.
(19) Duvenhage, D. J.; Coville, N. J. Fe: Co/TiO_2 Bimetallic Catalysts for the Fischer−Tropsch Reaction. Part 2. The Effect of Calcination and Reduction Temperature. *Appl. Catal., A* **2002**, *233*, 63−75.
(20) Li, J. L.; Coville, N. J. The Effect of Boron on the Catalyst Reducibility and Activity of Co/TiO_2 Fischer−Tropsch Catalysts. *Appl. Catal., A* **1999**, *181*, 201−208.
(21) Jalama, K.; Kabuba, J.; Xiong, H. F.; Jewell, L. L. Co/TiO_2 Fischer−Tropsch Catalyst Activation by Synthesis Gas. *Catal. Commun.* **2012**, *17*, 154−159.
(22) Zennaro, R.; Tagliabue, M.; Bartholomew, C. H. Kinetics of Fischer−Tropsch Synthesis on Titania-Supported Cobalt. *Catal. Today* **2000**, *58*, 309−319.
(23) Bartholomew, C. H.; Reuel, R. C. Cobalt Support Interactions - Their Effects on Adsorption and CO Hydrogenation Activity and Selectivity Properties. *Ind. Eng. Chem. Prod. Res. Dev.* **1985**, *24*, 56−61.
(24) Llorca, J.; Homs, N.; Sales, J.; de la Piscina, P. R. Efficient Production of Hydrogen over Supported Cobalt Catalysts from Ethanol Steam Reforming. *J. Catal.* **2002**, *209*, 306−317.
(25) Epling, W. S.; Cheekatamarla, P. K.; Lane, A. M. Reaction and Surface Characterization Studies of Titania-Supported Co, Pt and Co/Pt Catalysts for the Selective Oxidation of CO in H_2-Containing Streams. *Chem. Eng. J.* **2003**, *93*, 61−68.
(26) Brik, Y.; Kacimi, M.; Bozon-Verduraz, F.; Ziyad, M. Characterization and Comparison of the Activity of Boron-Modified Co/TiO_2 Catalysts in Butan-2-ol Conversion and Oxidative Dehydrogenation of Ethane. *J. Catal.* **2002**, *211*, 470−481.
(27) Riva, R.; Miessner, H.; Vitali, R.; Del Piero, G. Metal-Support Interaction in Co/SiO_2 and Co/TiO_2. *Appl. Catal., A* **2000**, *196*, 111−123.
(28) O'Shea, V. A. D.; Galvan, M. C. A.; Prats, A. E. P.; Campos-Martin, J. M.; Fierro, J. L. G. Direct Evidence of the SMSI Decoration Effect: The Case of Co/TiO_2 Catalyst. *Chem. Commun.* **2011**, *47*, 7131−7133.
(29) Shao, Y.; Chen, W.; Wold, E.; Paul, J. Dispersion and Electronic-Structure of TiO_2-Supported Cobalt and Cobalt Oxide. *Langmuir* **1994**, *10*, 178−187.
(30) Galhenage, R. P.; Ammal, S. C.; Yan, H.; Duke, A.; Tenney, S. A.; Heyden, A.; Chen, D. A. Nucleation, Growth and Adsorbate-Induced Changes in Composition for Co-Au Bimetallic Clusters on TiO_2. *J. Phys. Chem. C* **2012**, *116*, 24616−24629.
(31) Park, J. B.; Ratliff, J. S.; Ma, S.; Chen, D. A. Understanding the Reactivity of Oxide-Supported Bimetallic Clusters: Reaction of NO with CO on TiO_2(110)-Supported Pt-Rh Clusters. *J. Phys. Chem. C* **2007**, *111*, 2165−2176.
(32) Zhou, J.; Ma, S.; Kang, Y. C.; Chen, D. A. Dimethyl Methylphosphonate Decomposition on Titania-Supported Ni Clusters and Films: A Comparison of Chemical Activity on Different Ni Surfaces. *J. Phys. Chem. B* **2004**, *108*, 11633−11644.
(33) Park, J. B.; Conner, S. F.; Chen, D. A. Bimetallic Pt-Au Clusters on TiO_2(110): Growth, Surface Composition and Metal-Support Interactions. *J. Phys. Chem. C* **2008**, *112*, 5490−5500.
(34) Tenney, S. A.; Ratliff, J. S.; He, W.; Roberts, C. C.; Ammal, S. C.; Heyden, A.; Chen, D. A. Adsorbate-Induced Changes in the Surface Composition of Bimetallic Clusters: Au-Pt on TiO_2(110). *J. Phys. Chem. C* **2010**, *114*, 21652−21663.
(35) Tenney, S. A.; He, W.; Roberts, C. C.; Ratliff, J. S.; Shah, S. I.; Shafai, G. S.; Turkowski, V.; Rahman, T. S.; Chen, D. A. CO-Induced Diffusion of Ni Atoms to the Surface of Ni−Au Clusters on TiO_2(110). *J. Phys. Chem. C* **2011**, *115*, 11112−11123.
(36) Tenney, S. A.; Cagg, B. A.; Levine, M. S.; He, W.; Manandhar, K.; Chen, D. A. Enhanced Activity for Supported Au Clusters: Methanol Oxidation on Au/TiO_2(110). *Surf. Sci.* **2012**, *606*, 1233−1243.
(37) Mullins, D. R.; Overbury, S. H.; Huntley, D. R. Electron Spectroscopy of Single Crystal and Polycrystalline Cerium Oxide Surfaces. *Surf. Sci.* **1998**, *409*, 307−319.
(38) Mullins, D. R.; Zhang, K. Z. Metal-Support Interactions between Pt and Thin Film Cerium Oxide. *Surf. Sci.* **2002**, *513*, 163−173.
(39) Ozturk, O.; Ma, S.; Park, J. B.; Ratliff, J. S.; Zhou, J.; Mullins, D. R.; Chen, D. A. Probing the Interactions of Pt, Rh and Bimetallic Pt-

Rh Clusters with the TiO_2(110) Support. *Surf. Sci.* **2007**, *601*, 3099−3113.
(40) Chen, D. A.; Ratliff, J. S.; Hu, X.; Gordon, W. O.; Senanayake, S. D.; Mullins, D. R. Dimethyl Methylphosphonate Decomposition on Fully Oxidized and Partially Reduced Ceria Thin Films. *Surf. Sci.* **2010**, *604*, 574−587.
(41) Ratliff, J. S. The Morphology and Catalytic Activity of Bimetallic Nanoclusters Supported on TiO_2(110). PhD Dissertation, University of South Carolina, 2009.
(42) Hohenberg, P.; Kohn, W. Inhomogeneous Electron Gas. *Phys. Rev. B* **1964**, *136*, B854−B871.
(43) Kohn, W.; Sham, L. J. Self-Consistent Equations Including Exchange and Correlation Effects. *Phys. Rev.* **1965**, *140*, A1133−A1138.
(44) Kresse, G.; Furthmuller, J. Efficiency of Ab-Initio Total Energy Calculations for Metals and Semiconductors Using a Plane-Wave Basis Set. *Comput. Mater. Sci.* **1996**, *6*, 15−50.
(45) Kresse, G.; Furthmuller, J. Efficient Iterative Schemes for Ab Initio Total-Energy Calculations Using a Plane-Wave Basis Set. *Phys. Rev. B* **1996**, *54*, 11169−11186.
(46) Blochl, P. E. Projector Augmented-Wave Method. *Phys. Rev. B* **1994**, *50*, 17953−17979.
(47) Perdew, J. P.; Wang, Y. Accurate and Simple Analytic Representation of the Electron-Gas Correlation-Energy. *Phys. Rev. B* **1992**, *45*, 13244−13249.
(48) Islam, M. M.; Calatayud, M.; Pacchioni, G. Hydrogen Adsorption and Diffusion on the Anatase TiO_2(101) Surface: A First-Principles Investigation. *J. Phys. Chem. C* **2011**, *115*, 6809−6814.
(49) Finazzi, E.; Di Valentin, C.; Pacchioni, G.; Selloni, A. Excess Electron States in Reduced Bulk Anatase TiO_2: Comparison of Standard GGA, GGA Plus U, and Hybrid DFT Calculations. *J. Chem. Phys.* **2008**, *129*, 154113.
(50) Arroyo-de Dompablo, M. E.; Morales-Garcia, A.; Taravillo, M. DFT Plus U Calculations of Crystal Lattice, Electronic Structure, and Phase Stability under Pressure of TiO_2 Polymorphs. *J. Chem. Phys.* **2011**, *135*, 054503.
(51) Reddic, J. E.; Zhou, J.; Chen, D. A. Scanning Tunneling Microscopy Studies of the Growth of Cu Clusters on a Reconstructed TiO_2(110)-(1 × 2) Surface. *Surf. Sci.* **2001**, *494*, L767−L772.
(52) Zhou, J.; Chen, D. A. Controlling Size Distributions of Copper Islands Grown on TiO_2(110)-(1 × 2). *Surf. Sci.* **2003**, *527*, 183−187.
(53) Jak, M. J. J.; Konstapel, C.; van Kreuningen, A.; Chrost, J.; Verhoeven, J.; Frenken, J. W. M. The Influence of Substrate Defects on the Growth Rate of Palladium Nanoparticles on a TiO_2(110) Surface. *Surf. Sci.* **2001**, *474*, 28−36.
(54) Luo, K.; St. Clair, T. P.; Lai, X.; Goodman, D. W. Silver Growth on TiO_2(110) (1 × 1) and (1 × 2). *J. Phys. Chem. B* **2000**, *104*, 3050−3057.
(55) Gan, S.; Liang, Y.; Baer, D. R.; Grant, A. W. Effects of Titania Surface Structure on the Nucleation and Growth of Pt Nanoclusters on Rutile TiO_2(110). *Surf. Sci.* **2001**, *475*, 159−170.
(56) Valden, M.; Lai, X.; Goodman, D. W. Onset of Catalytic Activity of Gold Clusters on Titania with the Appearance of Nonmetallic Properties. *Science* **1998**, *281*, 1647−1650.
(57) Lai, X.; St. Clair, T. P.; Goodman, D. W. Oxygen-Induced Morphological Changes of Ag Nanoclusters Supported on TiO_2(110). *Faraday Discuss.* **1999**, *114*, 279−284.
(58) Chen, D. A.; Bartelt, M. C.; McCarty, K. F.; Hwang, R. Q. Self-Limiting Growth of Cu Islands on TiO_2(110). *Surf. Sci.* **2000**, *450*, 78−97.
(59) Zhou, J.; Kang, Y. C.; Chen, D. A. Controlling Island Size Distributions: A Comparison of Nickel and Copper Growth on TiO_2(110). *Surf. Sci.* **2003**, *537*, L429−L434.
(60) Xu, C.; Lai, X.; Zajac, G. W.; Goodman, D. W. Scanning-Tunneling-Microscopy Studies of the TiO_2(110) Surface: Structure and the Nucleation Growth of Pd. *Phys. Rev. B* **1997**, *56*, 13464−13482.
(61) Chen, D. A.; Seutter, S. M.; Bartelt, M. C.; McCarty, K. F. Small, Uniform, and Thermally Stable Silver Particles on TiO_2(110)-(1 × 1). *Surf. Sci.* **2000**, *464*, L708−L714.
(62) Park, J. B.; Ratliff, J. S.; Ma, S.; Chen, D. A. *In Situ* Scanning Tunneling Microscopy Studies of Bimetallic Cluster Growth: Pt-Rh on TiO_2(110). *Surf. Sci.* **2006**, *600*, 2913−2923.
(63) Jak, M. J. J.; Konstapel, C.; van Kreuningen, A.; Verhoeven, J.; Frenken, J. W. M. Scanning Tunneling Microscopy Study of the Growth of Small Palladium Particles on TiO_2(110). *Surf. Sci.* **2000**, *457*, 295−310.
(64) Berkó, A.; Klivényi, G.; Solymosi, F. Fabrication of Ir/TiO_2(110) Planar Catalysts with Tailored Particle Size and Distribution. *J. Catal.* **1999**, *182*, 511−514.
(65) Iddir, H.; Ögüt, S.; Browning, N. D.; Disko, M. M. Adsorption and Diffusion of Pt and Au on the Stoichiometric and Reduced TiO_2 Rutile (110) Surfaces. *Phys. Rev. B* **2005**, *72*, 081407.
(66) Chen, M. S.; Goodman, D. W. Catalytically Active Gold on Ordered Titania Supports. *Chem. Soc. Rev.* **2008**, *37*, 1860−1870.
(67) Masel, R. I. *Principles of Adsorption and Reaction on Solid Surfaces*; John Wiley and Sons, Inc.: New York, 1996.
(68) Bligaard, T.; Norskov, J. K.; Dahl, S.; Matthiesen, J.; Christensen, C. H.; Sehested, J. The Bronsted-Evans-Polanyi Relation and the Volcano Curve in Heterogeneous Catalysis. *J. Catal.* **2004**, *224*, 206−217.
(69) van Santen, R. A.; Neurock, M.; Shetty, S. G. Reactivity Theory of Transition-Metal Surfaces: A Bronsted-Evans-Polanyi Linear Activation Energy-Free-Energy Analysis. *Chem. Rev.* **2010**, *110*, 2005−2048.
(70) Evans, M. G.; Polyani, M. Inertia and Driving Force of Chemical Reactions. *Trans. Faraday Soc.* **1938**, *34*, 11−29.
(71) Bronsted, J. N. Acid and Basic Catalysis. *Chem. Rev.* **1928**, *5*, 231−338.
(72) Hammer, B.; Norskov, J. K. Theoretical Surface Science and Catalysis−Calculations and Concepts. In *Advances in Catalysis*; Academic Press Inc.: San Diego, 2000; Vol. *45*, pp 71−129.
(73) Norskov, J. K.; Bligaard, T.; Logadottir, A.; Bahn, S.; Hansen, L. B.; Bollinger, M.; Bengaard, H.; Hammer, B.; Sljivancanin, Z.; Mavrikakis, M.; et al. Universality in Heterogeneous Catalysis. *J. Catal.* **2002**, *209*, 275−278.
(74) Logadottir, A.; Rod, T. H.; Norskov, J. K.; Hammer, B.; Dahl, S.; Jacobsen, C. J. H. The Bronsted-Evans-Polanyi Relation and the Volcano Plot for Ammonia Synthesis over Transition Metal Catalysts. *J. Catal.* **2001**, *197*, 229−231.
(75) Pallassana, V.; Neurock, M. Electronic Factors Governing Ethylene Hydrogenation and Dehydrogenation Activity of Pseudomorphic Pd(ML)/Re(0001), Pd(ML)/Ru(0001), Pd(111), and Pd(ML)/Au(111) Surfaces. *J. Catal.* **2000**, *191*, 301−317.
(76) Liu, Z. P.; Hu, P. General Trends in CO Dissociation on Transition Metal Surfaces. *J. Chem. Phys.* **2001**, *114*, 8244−8247.
(77) Epling, W. S.; Peden, C. H. F.; Henderson, M. A.; Diebold, U. Evidence for Oxygen Adatoms on TiO_2(110) Resulting from O_2 Dissociation at Vacancy Sites. *Surf. Sci.* **1998**, *412−13*, 333−343.
(78) Du, Y. G.; Dohnalek, Z.; Lyubinetsky, I. Transient Mobility of Oxygen Adatoms Upon O_2 Dissociation on Reduced TiO_2(110). *J. Phys. Chem. C* **2008**, *112*, 2649−2653.
(79) Matthey, D.; Wang, J. G.; Wendt, S.; Matthiesen, J.; Schaub, R.; Laegsgaard, E.; Hammer, B.; Besenbacher, F. Enhanced Bonding of Gold Nanoparticles on Oxidized TiO_2(110). *Science* **2007**, *315*, 1692−1696.
(80) Hansen, J. O.; Lira, E.; Galliker, P.; Wang, J. G.; Sprunger, P. T.; Li, Z. S.; Laegsgaard, E.; Wendt, S.; Hammer, B.; Besenbacher, F. Enhanced Bonding of Silver Nanoparticles on Oxidized TiO_2(110). *J. Phys. Chem. C* **2010**, *114*, 16964−16972.
(81) Martinez, U.; Hammer, B. Adsorption Properties Versus Oxidation States of Rutile TiO_2(110). *J. Chem. Phys.* **2011**, *134*, 194703 .
(82) Pauling, L. *The Nature of the Chemical Bond*, 3rd ed.; Cornell University Press: New York, 1960.

(83) Mayer, J. T.; Diebold, U.; Madey, T. E.; Garfunkel, E. Titanium and Reduced Titania Overlayers on Titanium Dioxide(110). *J. Electron Spectrosc. Relat. Phenom.* **1995**, *73*, 1−11.
(84) Tenney, S. A.; He, W.; Ratliff, J. S.; Mullins, D. R.; Chen, D. A. Characterization of Pt-Au and Ni-Au Clusters on TiO_2(110). *Top. Catal.* **2011**, *54*, 42−45.
(85) Pesty, F.; Steinrück, H.-P.; Madey, T. E. Thermal Stability of Pt Films on TiO_2(110): Evidence for Encapsulation. *Surf. Sci.* **1995**, *339*, 83−95.
(86) Majzik, Z.; Balazs, N.; Berko, A. Ordered SMSI Decoration Layer on Rh Nanoparticles Grown on TiO_2(110) Surface. *J. Phys. Chem. C* **2011**, *115*, 9535−9544.
(87) Bowker, M.; Fourre, E. Direct Interactions between Metal Nanoparticles and Support: STM Studies of Pd on TiO_2(110). *Appl. Surf. Sci.* **2008**, *254*, 4225−4229.
(88) Bennett, R. A.; Stone, P.; Bowker, M. Pd Nanoparticle Enhanced Re-Oxidation of Non-Stoichiometric TiO_2: STM Imaging of Spillover and a New Form of SMSI. *Catal. Lett.* **1999**, *59*, 99−105.
(89) Bowker, M.; Stone, P.; Morrall, P.; Smith, R.; Bennett, R.; Perkins, N.; Kvon, R.; Pang, C.; Fourre, E.; Hall, M. Model Catalyst Studies of the Strong Metal-Support Interaction: Surface Structure Identified by STM on Pd Nanoparticles on TiO_2(110). *J. Catal.* **2005**, *234*, 172−181.
(90) Ozturk, O.; Park, J. B.; Black, T. J.; Rodriguez, J. A.; Hrbek, J.; Chen, D. A. Methanethiol Chemistry on TiO_2-Supported Ni Clusters. *Surf. Sci.* **2008**, *602*, 3077−3088.
(91) Dulub, O.; Hebenstreit, W.; Diebold, U. Imaging Surfaces with Atomic Resolution: The Strong Metal-Support Interaction State of Pt Supported TiO_2(110). *Phys. Rev. Lett.* **2000**, *84*, 3646−3649.
(92) Jennison, D. R.; Dulub, O.; Hebenstreit, W.; Diebold, U. Structure of an Ultrathin TiO_x Film, Formed by the Strong Metal Support Interaction (SMSI) on Pt Nanocrystals on TiO_2(110). *Surf. Sci.* **2001**, *492*, L677−L687.
(93) Wagner, C. D.; Riggs, W. M.; Davis, L. E.; Moulder, J. F. *Handbook of X-Ray Photoelectron Spectroscopy*; Perkin Elmer Corporation: Eden Prairie, MN, 1978.
(94) Chen, D. A.; Friend, C. M. Adsorbate-Induced Structural Changes of Metal Thin Films: Cobalt-Oxygen and Cobalt-Sulfur Overlayers on Mo(110). *Surf. Sci.* **1997**, *371*, 131−142.
(95) Parteder, G.; Allegretti, F.; Surnev, S.; Netzer, F. P. Growth of Cobalt on a V0(111) Surface: Template, Surfactant or Encapsulant Role of the Oxide Nanolayer? *Surf. Sci.* **2008**, *602*, 2666−2674.
(96) Schneider, C. M.; Pracht, U.; Kuch, W.; Chasse, A.; Krischner, J. Magnetic Dichroism in Photoemission as a Spin-Resolving Probe for Electronic Correlations. *Phys. Rev. B* **1996**, *54*, 15618−15621.
(97) Nath, K. G.; Haruyama, Y.; Kinoshita, T. Observation of the Satellite Signal in Co 2p Photoemission Spectra: Evidence of a Localized Electronic Structure in Thin Films. *Phys. Rev. B* **2001**, *64*, 245417.
(98) Nath, K. G.; Haruyama, Y.; Kinoshita, T. Surface Superstructure Formation, Electronic Structure Modification and Magnetic Stability of Co Films on Oxygen-Rich Cu(001): Confirmation of Oxygen-Surfactant Effect. *Surf. Sci.* **2001**, *486*, 185−193.
(99) Chen, C. F. Novel Many-Body Effects in the Photoemission Spectrum of Ultrathin BCC Cobalt Films. *Phys. Rev. Lett.* **1990**, *64*, 2176−2179.
(100) Chen, C. F. Photoemission as a Probe of Electronic States in Ultrathin Magnetic Overlayers−Correlation and Hybridization Effects. *Phys. Rev. B* **1993**, *48*, 1318−1321.
(101) Santra, A. K.; Yang, F.; Goodman, D. W. The Growth of Ag-Au Bimetallic Nanoparticles on TiO_2(110). *Surf. Sci.* **2004**, *548*, 324−332.
(102) Kitchin, J. R.; Barteau, M. A.; Chen, J. G. G. A Comparison of Gold and Molybdenum Nanoparticles on TiO_2(110) 1 × 2 Reconstructed Single Crystal Surfaces. *Surf. Sci.* **2003**, *526*, 323−331.
(103) Berko, A.; Magony, A.; Szoko, J. Characterization of Mo Deposited on a TiO_2(110) Surface by Scanning Tunneling Microscopy and Auger Electron Spectroscopy. *Langmuir* **2005**, *21*, 4562−4570.
(104) Lai, X.; Xu, C.; Goodman, D. W. Synthesis and Structure of Al Clusters Supported on TiO_2(110): A Scanning Tunneling Microscopy Study. *J. Vac. Sci. Technol., A* **1998**, *16*, 2562−2566.
(105) Pan, J. M.; Maschhoff, B. L.; Diebold, U.; Madey, T. E. Structural Study of Ultrathin Metal Films on TiO_2 Using LEED ; ARXPS and MEED. *Surf. Sci.* **1993**, *291*, 381−394.
(106) Zhang, L.; Persaud, R.; Madey, T. E. Ultrathin Metal-Films on a Metal-Oxide Surface: Growth of Au on TiO_2(110). *Phys. Rev. B* **1997**, *56*, 10549−10557.
(107) Pan, J. M.; Diebold, U.; Zhang, L. Z.; Madey, T. E. Ultrathin Reactive Metal-Films on TiO_2(110): Growth; Interfacial Interaction and Electronic Structure of Chromium Films. *Surf. Sci.* **1993**, *295*, 411−426.
(108) Diebold, U.; Shinn, N. D. Adsorption and Thermal Stability of Mn on TiO_2(110): 2p X-Ray-Absorption Spectroscopy and Soft-X-Ray Photoemission. *Surf. Sci.* **1995**, *343*, 53−60.
(109) Overbury, S. H. Surface composition of binary systems. Prediction of surface phase diagrams of solid solutions. *Chem. Rev.* **1975**, *75*, 547−560.
(110) Tanaka, K.; Tamaru, K. A General Rule in Chemisorption of Gases on Metals. *J. Catal.* **1963**, *2*, 366−370.
(111) Diebold, U.; Tao, H. S.; Shinn, N. D.; Madey, T. E. Electronic-Structure of Ultrathin Fe Films on TiO_2(110) Studied with Soft X-Ray Photoelectron Spectroscopy and Resonant Photoemission. *Phys. Rev. B* **1994**, *50*, 14474−14480.
(112) Zhang, Z.; Henrich, V. E. Electronic Interactions in the Vanadium/TiO_2(110) and Vanadia/TiO_2(110) Model Catalyst System. *Surf. Sci.* **1992**, *277*, 263−272.
(113) Domenichini, B.; Petigny, S.; Blondeau-Patissier, V.; Steinbrunn, A.; Bourgeois, S. Effect of the Surface Stoichiometry on the Interaction of Mo with TiO_2 (110). *Surf. Sci.* **2000**, *468*, 192−202.
(114) Domenichini, B.; Blondeau-Patissier, V.; Casanove, M. J.; Lian, G. D.; Bourgeois, S. Effect of the Mo Atom Flow on the Molybdenum Growth on TiO_2(110) Surface. *J. Cryst. Growth* **2004**, *263*, 256−262.
(115) Mendes, F. M. T.; Uhl, A.; Starr, D. E.; Guimond, S.; Schmal, M.; Kuhlenbeck, H.; Shaikhutdinov, S. K.; Freund, H. J. Strong Metal Support Interaction on Co/Niobia Model Catalysts. *Catal. Lett.* **2006**, *111*, 35−41.
(116) Law, Y. T.; Skala, T.; Pis, I.; Nehasil, V.; Vondracek, M.; Zafeiratos, S. Bimetallic Nickel-Cobalt Nanosized Layers Supported on Polar ZnO Surfaces: Metal-Support Interaction and Alloy Effects Studied by Synchrotron Radiation X-Ray Photoelectron Spectroscopy. *J. Phys. Chem. C* **2012**, *116*, 10048−10056.
(117) Hyman, M. P.; Martono, E.; Vohs, J. M. Studies of the Structure and Interfacial Chemistry of Co Layers on ZnO(0001). *J. Phys. Chem. C* **2010**, *114*, 16892−16899.
(118) Su, S. H.; Lai, J. H.; Chen, H. H.; Lee, T. H.; Hsu, Y. J.; Wang, R. L.; Huang, J. C. A. Elucidating the Structure and Chemical State of Co Growth on the ZnO($10\bar{1}0$) Surface. *J. Phys. Chem. C* **2012**, *116*, 9917−9924.
(119) Carlsson, A. F.; Baumer, M.; Risse, T.; Freund, H. J. Surface Structure of Co-Pd Bimetallic Particles Supported on Al_2O_3 Thin Films Studied Using Infrared Reflection Absorption Spectroscopy of CO. *J. Chem. Phys.* **2003**, *119*, 10885−10894.
(120) Hill, T.; Mozaffari-Afshar, M.; Schmidt, J.; Risse, T.; Stempel, S.; Heemeier, M.; Freund, H. J. Influence of CO Adsorption on the Magnetism of Small Co Particles Deposited on Al_2O_3. *Chem. Phys. Lett.* **1998**, *292*, 524−530.
(121) *CRC Handbook of Chemistry and Physics*, 67th ed.; Weast, R. C., Ed.; CRC Press, Inc.: Boca Raton, FL, 1986−1987.